Available online at www.sciencedirect.com
ScienceDirect
Trans. Nonferrous Met. Soc. China 25(2015) 3634−3642
Transactions of Nonferrous Metals Society of China
www.tnmsc.cn

Photocatalytic activity of CuO nanoparticles incorporated in mesoporous structure prepared from bis(2-aminonicotinato) copper(II) microflakes

Azadeh TADJARODI[1], Omid AKHAVAN[2,3], Keyvan BIJANZAD[1]

1. Research Laboratory of Inorganic Materials Synthesis, Department of Chemistry, Iran University of Science and Technology, Tehran 16846-13114, Iran;
2. Department of Physics, Sharif University of Technology, Tehran 11155-9161, Iran;
3. Institute for Nanoscience and Nanotechnology, Sharif University of Technology, Tehran 14588-89694, Iran

Received 7 December 2014; accepted 18 June 2015

Abstract: An easy method for preparing CuO nanoparticles incorporated in a mesoporous structure was presented based on the thermal decomposition of a copper complex. The novel copper coordination compound of $[Cu(anic)_2]\cdot 0.75H_2O$ (anic= 2-aminonicotinate) with the microflake morphology was synthesized through the reaction of 2-aminonicotinic acid (Hanic) and copper(II) nitrate. Using elemental analysis and Fourier transform infrared (FTIR) spectroscopy, the chemical composition of $CuC_{12}H_{11.5}N_4O_{4.75}$ was proposed. Calcination process at 550 °C for 4 h transformed the microflakes into CuO nanoparticles incorporated in a mesoporous structure. The FTIR peaks assigned to 2-aminonicotinate were completely removed after calcination, confirming CuO formation. X-ray diffraction (XRD) analysis also confirmed the generation of pure and crystalline CuO. SEM showed CuO nanoparticles with the average diameter of 75 nm. The diffuse reflectance spectrum (DRS) of the CuO nanoparticles showed a band gap energy of ~1.58 eV. The degradation efficiency toward rhodamine B was almost 100 % after 5 h illumination when both CuO and H_2O_2 were utilized. The results show that the product can be used as an efficient photocatalyst for water treatment.

Key words: copper oxide; nanostructure; 2-aminonicotinic acid; photocatalyst; thermal decomposition; degradation efficiency

1 Introduction

The nanostructures of CuO, as a p-type semiconductor with narrow band gaps of 1.2−1.4 eV [1−4], have widely been used as catalysts [5,6], ultraviolet and/or visible light-driven photocatalysts [7−12], antibacterial materials [13−15], lithium ion batteries [16] and biosensors [17]. The physicochemical properties of CuO nanomaterials strictly depend on their size and morphology [18,19]. Hence, lots of efforts have been carried out to prepare various nanostructures. So far, numerous morphologies of copper oxide nanostructures have been synthesized and reported [20−23]. For example, it was reported that $Cu(OH)_2$ could maintain the initial nanowire morphology during the chemical transformation into CuO applied in more active electrochemical reactions [24]. Nanowhisker-like CuO thin films with high photocatalytic activity were prepared by electrochemical route [25]. Morphologies such as leaf-like, oatmeal-like and hollow spherical CuO were also synthesized by solution and hydrothermal reactions [26]. A gradual transformation from Cu_2O to CuO one-dimensional nanostructures was observed by increasing the deposition temperature in CVD process utilizing β-diketonate diamine precursor [27]. Additionally, CuO nanocubes, nanorods and nanosheets were synthesized using tetraoctylammonium bromide as a surfactant in a wet chemical method [28].

A well-known and low-cost method for preparing metal oxide nanostructures with high purity is the thermal decomposition of precursors. Concerning this, rod-shaped CuO nanoparticles were synthesized by direct thermal decomposition of $[Cu_4(SO_4)(OH)_6]$ [13]. Nanosized three-dimensional supramolecular, $[Cu(L)_2\cdot(H_2O)_2]$ (L=1H-1,2,4-triazole-3-carboxylate), was synthesized by sonochemical process and subsequent calcination process yielded CuO nanoparticles [29]. High specific surface area (>70 m^2/g) of CuO was also reported by the decomposition of copper(II) oxalate where the use of hydroxylpropylmethylcellulose polymer was responsible for the

Corresponding author: Azadeh TADJARODI; Tel: +98-21-77240516; Fax: +98-21-77491204; E-mail: tajarodi@iust.ac.ir
DOI: 10.1016/S1003-6326(15)64004-3

cubic morphology and large specific surface area [30]. The possibility to obtain pure metal oxide nanostructures from metal complexes paves the way to connect coordination science and nanotechnology. In fact, coordination compounds with different kinds of ligands are suitable candidates to prepare metal oxide nanostructures [31−33]. On the other hand, due to the specific topology of 2-aminonicotinic acid, it is potentially capable of coordinating to the metals through carboxylic acid groups or via two distinct amine sites. For example, this ligand acted as a light collector in the structure of the photoluminescent $[Tb(anic)_3]\cdot 0.5Hanic\cdot 7H_2O$ [34]. Ag_2-μ-O, O′$(anic)_2$-$(NO_3)_2]_n$ with considerable antibacterial activities against *Ps. Aeruginosa* is another sample of Hanic coordination compounds [35]. In the structure of $[TlMe_2(anic)]_n$, the ligand played the role of a bridge to link two $[TlMe_2]^+$ moieties, via two oxygen atoms of the carboxylate group and the pyridine nitrogen atom [36]. To the best of our knowledge, there are no reports on the synthesis of CuO nanostructures by thermal decomposition of copper complex with 2-aminonicotinic acid.

In this research, at first, the novel coordination compound of $CuC_{12}H_{11.5}N_4O_{4.75}$ with microflake morphology was synthesized through a solution precipitation method. Then, the synthesized 2-amino-nicotinate copper complex microflakes were used as a precursor to prepare CuO nanoparticles by thermal decomposition. The products were characterized by elemental analysis, FTIR and UV–Vis spectroscopies, XRD, scanning electron microscopy (SEM) and BET N_2 adsorption−desorption analysis.

2 Experimental

2.1 Chemicals and synthesis

All of the reagents were purchased from the Merck Company and used without further purification. A KOH aqueous solution (2 mmol KOH in 30 mL deionized (DI) water) was added into a 2-aminonicotinic acid solution (2 mmol in 30 mL ethanol) until the pH of the total solution was 7, measured by a Metrohm pH meter. A copper(II) nitrate trihydrate aqueous solution (1 mmol in 20 mL DI water) was then added dropwise to this solution while stirring for 30 min. It gave the green precipitate of copper coordination compound (with a melting point of ~280 °C) which was then filtered, washed and dried at room temperature during the night. The coordination compound, as a precursor, was calcined at 550 °C in air for 4 h to prepare CuO nanoparticles. A schematic representation of the reaction is shown as follows:

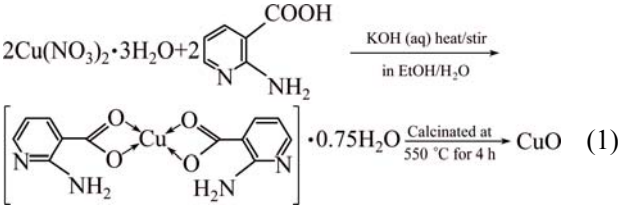

(1)

2.2 Characterization

The powder X-ray diffraction measurement was performed using a JEOL diffractometer with monochromatic Cu K_α radiation (λ=1.5418 Å). Rapid Heraeus elemental analyzer was used to perform elemental analysis. Diffuse reflectance spectra (DRS) were obtained by a Shimadzu (MPC–2200) spectro-photometer. FTIR spectra were recorded on a Shimadzu−8400S spectrometer in the wavenumber range of 400−4000 cm^{-1} using KBr pellets. SEM images were taken by a VEGA/TESCAN microscope at an accelerating voltage of 30 kV. The surface area of the product was obtained using the Brunauer−Emmett−Teller (BET) technique with micromeritics (Gemini) in the relative pressures range of 0.0−1.0. The sample was degassed at 473 K for 2 h, before measurement. Furthermore, the pore size distribution was determined from the desorption branch of the isotherm curve using the Barrett−Joyner−Halenda (BJH) model. The UV−Vis absorption study was performed at room temperature in the wavelength range of 190−800 nm on a UV−Vis spectrophotometer (Shimadzu UV−1700). The pH was measured by a Metrohm pH meter type 1.712.0010 that was purchased from Metrohm Herisau, Switzerland.

2.3 Photocatalytic test

Rhodamine B (RhB) was used as the representative pollutant to evaluate the photocatalytic activity of the produced CuO. The photodegradation experiments were carried out under the following conditions: 0.05 g CuO nanoparticles as the photocatalyst were added into a 100 mL dye aqueous solution with the initial concentration of 10 mg/L at room temperature and neutral pH, followed by addition of 1.5 mL H_2O_2. The resultant suspension was stirred using a magnetic stirrer for 1 h in dark to establish an adsorption−desorption equilibrium. The concentration of the residual dye was measured using UV–Vis spectrophotometer at proper wavelength that corresponds to the maximum absorption of RhB (554 nm). The reaction vessel was subjected to light irradiation in the photo-reactor to continue the photodegradation process. Light irradiation was supplied by a 500 W high-pressure mercury-vapor lamp (λ= 546.8 nm) that was mounted 10 cm from the reaction solution. The mercury lamp (HWL, 500 W, 225 V, E40) was purchased from the OSRAM Company in China and

the short-wavelength components of the supplied light (λ=350 nm) were cut off using a filter. At given irradiation time intervals, the portions of the suspension were taken from the reaction vessel, centrifuged at 14000 r/min for 5 min and analyzed by UV–Vis spectrophotometer.

3 Results and discussion

3.1 Compositional characterization, morphological and optical studies

The elemental analysis was utilized to determine the mass fractions of carbon, hydrogen and nitrogen in the composition of the copper complex. It verified the product of a copper coordination compound for which the empirical formula of $CuC_{12}H_{11.5}N_4O_{4.75}$ was proposed. The calculated mass fractions of elements for $CuC_{12}H_{11.5}N_4O_{4.75}$ are as follows: 40.48% C; 3.21% H; 15.63% N. The measured mass fractions of elements for $CuC_{12}H_{11.5}N_4O_{4.75}$ are as follows: 41.02% C; 3.28% H; 15.95% N.

The FTIR spectra of the complex and the copper oxide nanostructures are shown in Figs. 1(a_1) and (a_2), respectively. All the corresponding peaks of the ligand functional groups were present in the spectrum of $[Cu(anic)_2]\cdot 0.75H_2O$[34]. Aromatic C—H bending vibrations were seen at 688−840 cm^{-1}. The bands originated from the N—C and C—O vibrations were observed at ~1257 cm^{-1}. The peaks at 1500 and 1550 cm^{-1} were ascribed to the C═C stretching and N—H bending vibrations, respectively. The peaks at 3159 and 3319, and ~3400 cm^{-1} were representative for water molecules and amine group, respectively. In the complex, there was no shift to lower wavenumbers for amine peaks after coordination, suggesting that the ligand was not coordinated to metal through the nitrogen atoms of amine group. Asymmetric vibrational mode of the carboxylate group in the complex shifted to lower wavenumbers (at 1672 cm^{-1}) and the symmetric vibrational mode shifted to higher wavenumbers (at 1658 cm^{-1}), as compared with free ligand, anic, located at 1704 and 1548 cm^{-1}, respectively. These shifts implied coordination through carboxylate group [34,37]. It was suggested that in the structure of copper complex, the ligand was coordinated to copper via the two oxygen atoms of the carboxylate groups which might in turn participate in hydrogen bonding. All the characteristic peaks of the ligand disappeared after calcination process and only the peaks at 530 and 578 cm^{-1} remained, which was attributed to the Cu—O bond (Fig. 1(a_2)).

XRD was used to clarify the CuO phase formation. All the reflections were well indexed to monoclinic phase of CuO (JCPDS card No. 00−045−0937). As it can be seen from Fig. 1(b), the diffraction peaks at 2θ values of 35.40°, 38.73°, 48.73°, 53.45°, 58.34°, 61.53°, 66.25° and 68.09° match the respective (002), (111), $(\bar{2}02)$, (020), (202), $(\bar{1}13)$, $(\bar{3}11)$ and $(\bar{2}20)$ planes of monoclinic CuO with a space group of $C2/c$ and lattice parameters of a=4.68 Å, b=3.43 Å and c=5.13 Å, α=90°, β=99.55° and γ=90° are obtained. The excellent crystallinity and absence of impurities can be inferred as a result of sharpness and exact number of peaks in the XRD pattern. Additionally, it indicates that the product is a single phase.

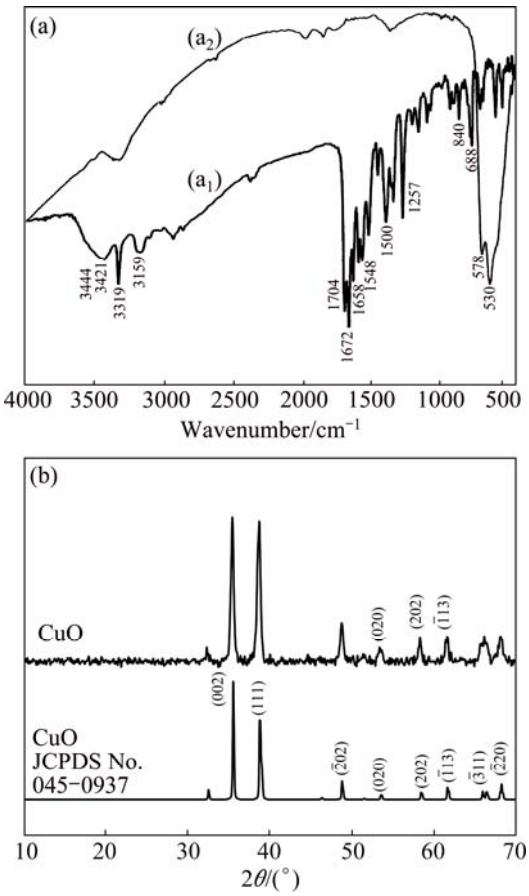

Fig. 1 FTIR spectra of copper complex (a_1) and CuO nanostructure (a_2) and XRD patterns of CuO nanostructure and standard CuO (JCPDS card No. 045−0937) (b)

SEM was used to study the size and morphology of the products. It is obvious in Figs. 2(a,b) that the copper complex consisted of distinct microflakes with lateral dimensions of ~2.92 μm and thickness of ~685 nm. A porous structure of CuO nanoparticles (with average particle size of ~75 nm) was produced after calcination step, as clearly seen in Figs. 2(c) and (d). The average size of the nanoparticles was determined using the microstructure measurement program and Minitab statistical software. The histogram of the particle size distribution according to SEM images is illustrated in Fig. 2(e). It is concluded that during thermal decomposition of the complex, volatile gases, i.e., carbon

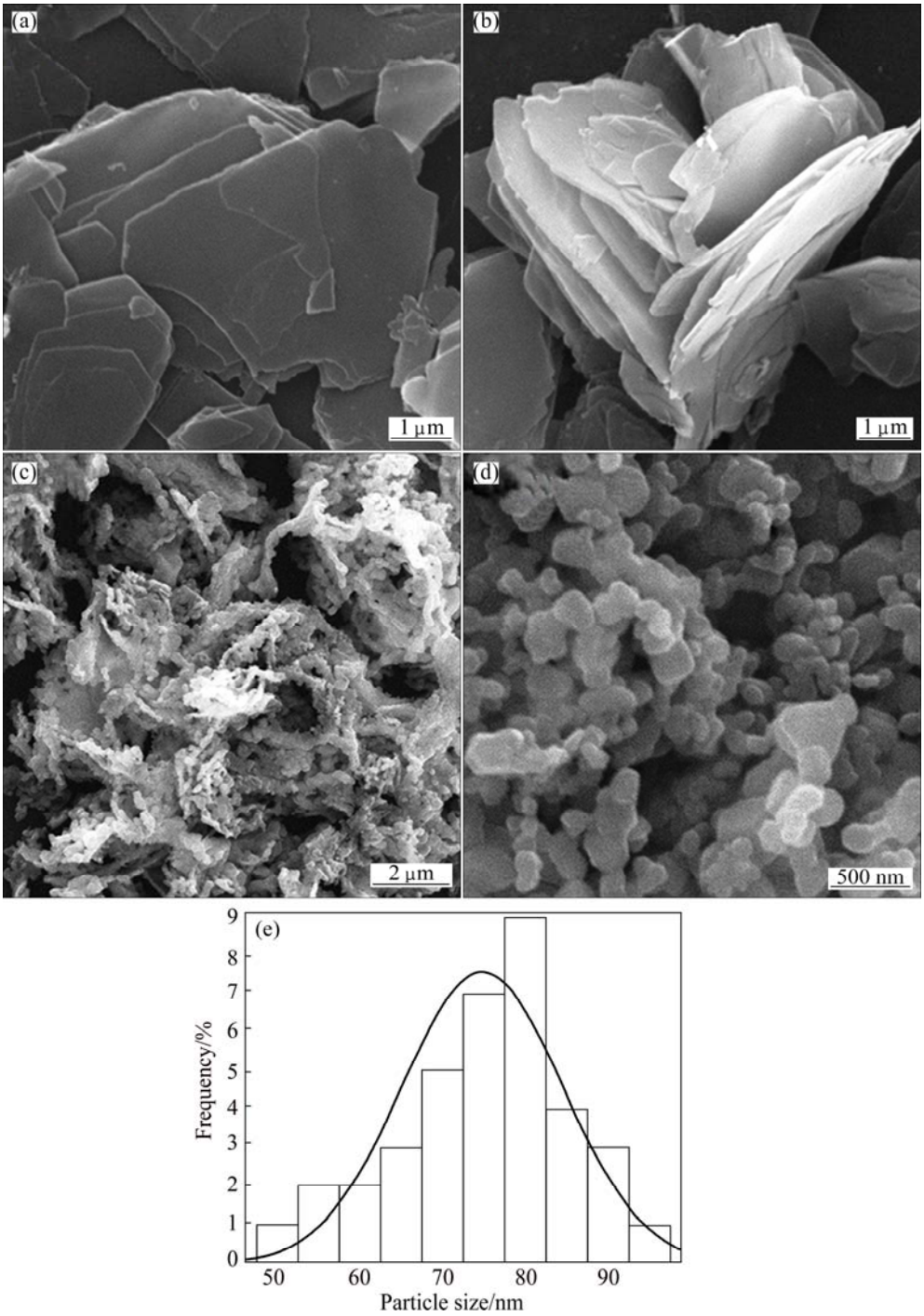

Fig. 2 SEM images of copper complex microflakes (a,b), CuO nanoparticles (c,d) and histogram graph of particle size distribution (e)

dioxide, water vapor and nitrogen oxides were released. Since the decomposition and boiling points of the organic compounds are lower than those of inorganic metal oxides, when a coordination compound is calcined, at first, the organic section of the complex (containing C, H, N and O) will be decomposed and released. The metal oxides resulting from the metal complexes have ultra-high boiling points which are higher than the calcination temperature. Thus, after the calcination process, the only remained precipitate will be the copper oxide. Consequently, a morphological evolution from continuous microflakes to porous structure of CuO nanoparticles occurred. It is believed that the gas liberation (carbon dioxide, water vapor and nitrogen oxides from the organic section of the complex) is mainly responsible for the formation of CuO nanoparticles.

Figure 3(a_1) shows the nitrogen adsorption−desorption isotherm and the corresponding pore size distribution curve of the CuO nanostructure using the

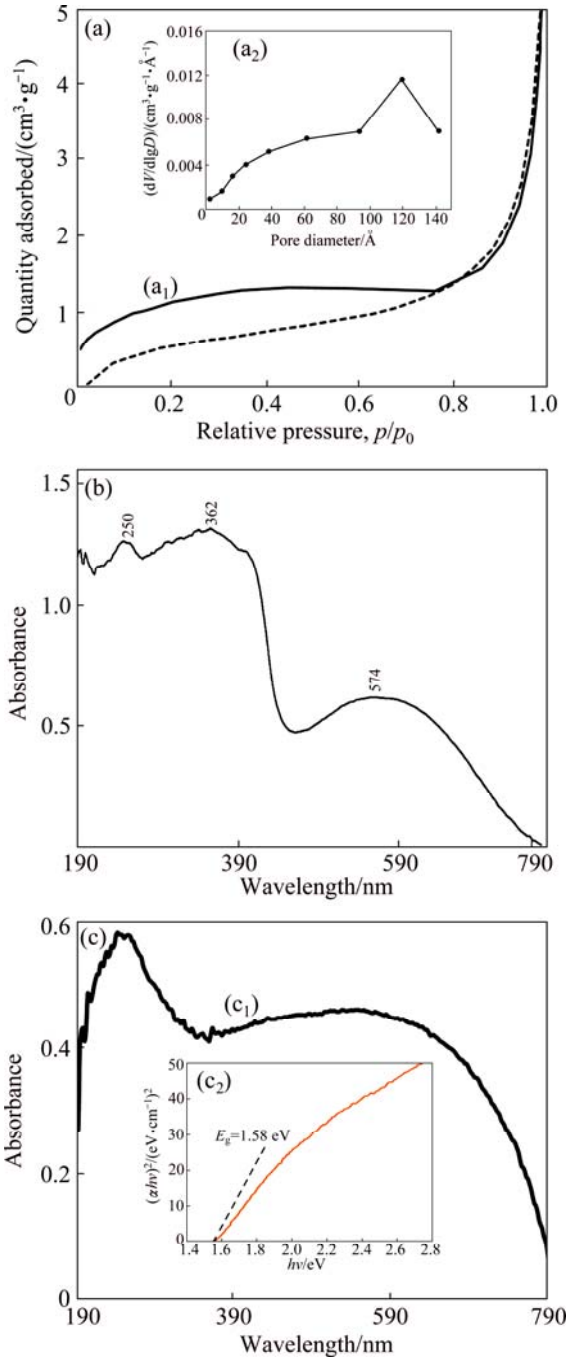

Fig. 3 Nitrogen adsorption (full line) and desorption (dashed line) isotherms for CuO nanoparticles (a_1) and BJH plot of product (a_2), DRS of copper complex (b); DRS of CuO nanoparticles (c_1) and plot of $(\alpha hv)^2$ vs hv for CuO nanoparticles (c_2)

Barrett–Joyner–Halenda (BJH) model. A hysteresis loop in the range of $0<p/p_0<1$ corresponding to diagram V with an H3 type loop is clearly observed which clarifies the presence of mesopores in the CuO nanostructures. The existence of mesopores is further confirmed by the corresponding pore size distribution (Fig. 3(a_2)). The Brunauer−Emmett−Teller (BET) surface area was calculated to be 4.20 m^2/g. Although the sizes of mesopores are not uniform, they are centered at 12.33 nm.

To study electron transitions in the structure of the copper complex and copper oxide nanostructures, optical absorption spectroscopy was carried out. Figure 3(b) shows that there are three peaks in the DRS of the complex. The first two peaks with high intensities at 250 and 362 nm were ascribed to the transition of electron from π to π* and n to π* molecular orbitals of the ligand section, respectively. The weak peak at 574 nm was assigned to the electronic transition from d to d metal orbitals of the complex which was a good evidence for the presence of copper in the composition [38]. The DRS of CuO (Fig. 3(c_1)) revealed broad absorption bands ranging from ultraviolet to visible regions (200−800 nm). The optical absorption data near the band edge were utilized to calculate the band gap of the product using the following equation:

$$\alpha hv=A(hv-E_g)^{n/2} \quad (1)$$

where α, v, A and E_g are the absorption coefficient, light frequency, proportionality constant and band gap energy, respectively. Here, n identifies whether the transition in a semiconductor is direct (n=1) or indirect (n=4). The values of n and E_g can be estimated as follows: 1) presuming an approximate E_g value, $\ln(\alpha hv)$ vs $\ln(hv-E_g)$ should be plotted, and the value of n can be obtained from the slope of the straightest line near the band edge; 2) $(\alpha hv)^{2/n}$ vs hv should be plotted, and the band gap energy E_g can be calculated by extrapolating the straightest line to the hv axis intercept [39]. Using the plot of $(\alpha hv)^2$ vs hv (Fig. 3(c_2)) obtained from the optical absorption spectrum of CuO (Fig. 3(c_1)), the band gap energy of CuO was calculated to be ~1.58 eV. The most conventional reported band gap energy for CuO was 1.2 eV [40], but because of different morphologies, its range in the literature is reported to be from 1.2 to 2.71 eV, for example, 1.37 and 1.39 eV, respectively for the as-synthesized and annealed films at 300 °C [41] and 2.71 eV for porous CuO hollow microspheres [42].

3.2 Photocatalytic activity

3.2.1 Photocatalytic experiment

The photocatalytic activity of the CuO nanoparticles was investigated by the degradation of toxic dye of RhB from aqueous solution. The removal efficiency (η) is calculated by the following equation:

$$\eta=\frac{c_0-c_t}{c_0}\times 100\% \quad (2)$$

where c_0 is the initial concentration of dye and c_t is the concentration of dye after treatment at different time intervals, t (0−5 h). The control tests revealed that the maximum RhB removal efficiency, after 5 h of

illumination, was 100% when 0.05 g of CuO was applied along with 1.5 mL of H_2O_2.

Only very little adsorption of the dye pollutant was observed when CuO was used without H_2O_2. The removal efficiency was 66.24% after 5 h in the case of H_2O_2, and when both CuO and H_2O_2 were applied, photocatalytic efficiency was almost 100% after 5 h illumination as shown in Fig. 4(a). As it is obvious in Fig. 4(b) that, most of photodegradation occurred in the first 1 h of addition of H_2O_2 to photocatalyst, therefore, it can be concluded that H_2O_2 could successively activate copper oxide and trigger the photocatalysis process.

Figure 4(c) showed that there was not great difference in the adsorption process of CuO, and CuO and H_2O_2 in the dark, so, H_2O_2 did not change the structure or porosity of CuO.

3.2.2 Photocatalytic reaction kinetics

To evaluate the kinetics of photocatalysis, the decolorization rate of RhB dye was recorded at different time. A linear relationship between ln (c_0/c_t) vs reaction time, t, was observed (Fig. 4(c)), which is indicative of a pseudo-first-order kinetic model (Eq. 3) for the photocatalytic degradation process by CuO, and CuO and H_2O_2.

$$\ln(c_0/c_t)=kt \quad (3)$$

where c_0 is the initial concentration (mmol/L), c_t is the instantaneous concentration of the dye in different intervals of illumination, and the slope, k, is the apparent rate constant. From the diagrams, the rate constants of photodegradation reactions for RhB dye by CuO and CuO and H_2O_2 were 0.0082 and 0.0034 min^{-1}, respectively.

3.2.3 Photodegradation mechanism

The photocatalytic activity is mainly originated from strong oxidizing agents such as hydroxyl ($^{\bullet}OH$) and superoxide ($O_2^{\bullet-}$) radicals. They result from the formation of electron/hole pairs as a consequence of light irradiation. When the dye molecules are illuminated, they would be excited and the electrons transfer to the conduction band of the photocatalyst. The produced dye radicals react on the surface of the catalyst to give oxygen radicals such as $O_2^{\bullet-}$, H_2O_2 and $O_2^{\bullet}$.

The decolorization rate would increase in the presence of H_2O_2 which occurs as a consequence of the produced hydroxyl radicals through absorbing light [43]. H_2O_2 as an oxidizing agent has various advantages such as commercial availability, thermal stability and infinite

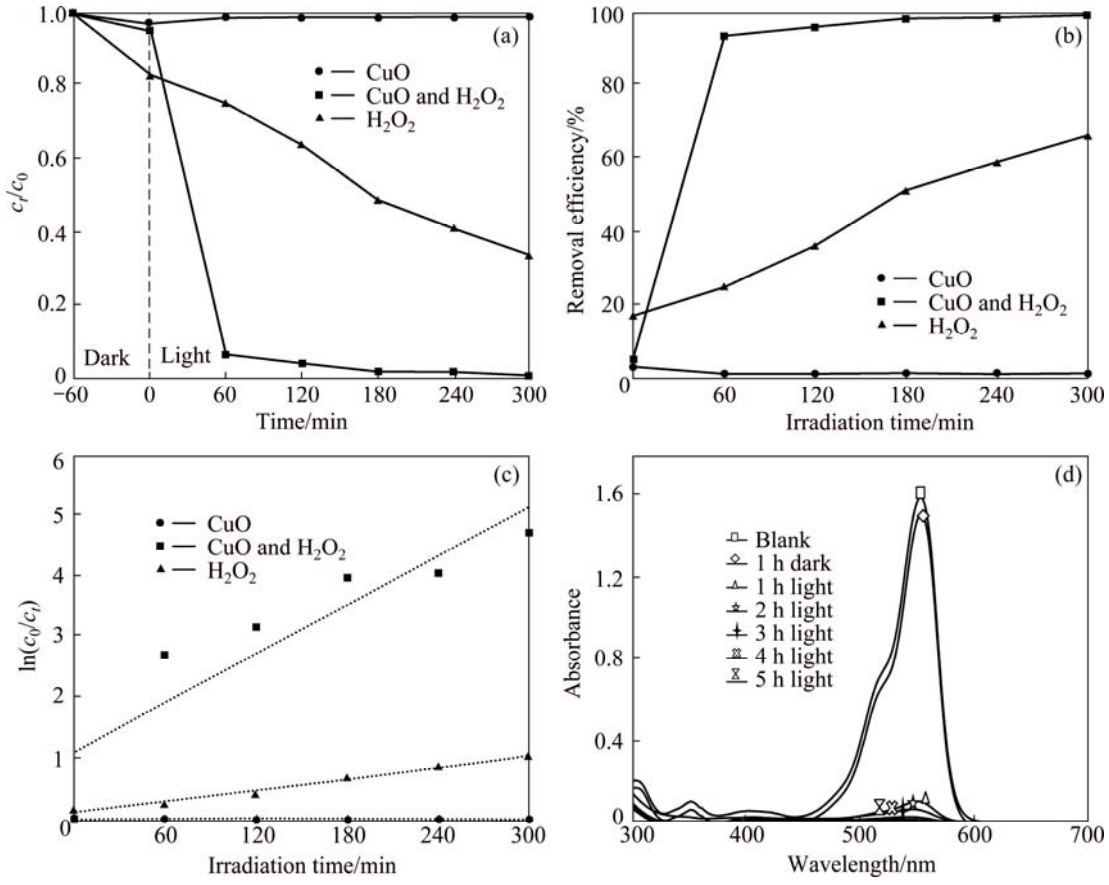

Fig. 4 Comparison of photocatalytic degradation of RhB in presence of CuO, CuO and H_2O_2, and H_2O_2 (a), removal efficiency of CuO, CuO and H_2O_2, and H_2O_2 toward RhB dye solution over 5 h (b), photocatalytic kinetics for degradation of RhB molecules after light illumination (c), UV absorption spectra of RhB in the presence of 0.05 g CuO and 1.5 mL H_2O_2 upon light illumination for 5 h (d)

solubility in water. The common mechanism for the photolysis of H_2O_2 is its cleavage into hydroxyl radicals. The $^{\bullet}OH$ radicals undergo radical-chain reaction with the pollutant molecules forming intermediates, which react with $^{\bullet}OH$ radicals to be mineralized, ultimately. It is noteworthy that increasing H_2O_2 concentration has two opposite effects: 1) As the concentration of H_2O_2 is increased, more hydroxyl radicals will be produced to attack the aromatic rings and hence the rate of reaction increases; 2) When H_2O_2 is used in excess, hydroxyl radical will react with H_2O_2 and produce $HO_2^{\bullet}$, also $^{\bullet}OH$ radicals are generated at high concentration, dimerize to H_2O_2. Also, the hydrogen peroxide would accept the photogenerated electrons from the conduction band to form hydroxyl radicals, thus preventing the recombination of charges. In addition, H_2O_2 may shift the absorption spectrum of the photocatalyst towards the visible region by the formation of complexes on its surface, and furthermore, it produces O_2 during its photochemical reactions. The photochemical reaction occurred by the photocatalyst, broke down the dye pollutants to CO_2, H_2O and inorganic acids which were no more toxic [44,45].

4 Conclusions

1) The coordination compound of $[Cu(anic)_2]\cdot 0.75H_2O$ was synthesized with microflake morphology by the reaction of Hanic and copper (II) nitrate trihydrate. In this structure, the ligand was coordinated to the metal center through the carboxylate group in a bidendate mode.

2) Calcination of the copper complex microflakes at 550 °C for 4 h made CuO nanoparticles incorporated in a mesoporous structure. No additional purification treatments such as washing and/or heating are required for the nanoparticles in this method. These features make this method an easy technique to prepare high crystalline and purified CuO nanoparticles.

3) The produced CuO showed a very good photocatalytic performance against RhB dye molecules.

Acknowledgments

The authors would like to thank Iran University of Science and Technology, the Research Council of Sharif University of Technology and Iran Nanotechnology Initiative Council for financial support of this work.

References

[1] RAFEA M A, ROUSHDY N. Determination of the optical band gap for amorphous and nanocrystalline copper oxide thin films prepared by SILAR technique [J]. Journal of Physics D: Applied Physics, 2009, 42: 1−6.

[2] AKHAVAN O, TOHIDI H, MOSHFEGH A Z. Synthesis and electrochromic study of sol−gel cuprous oxide nanoparticles accumulated on silica thin film [J]. Thin Solid Films, 2009, 517: 6700−6706.

[3] ORAL A Y, MENŞUR E, ASLAN M H, BAŞARAN E. The preparation of copper(II) oxide thin films and the study of their microstructures and optical properties [J]. Materials Chemistry and Physics, 2004, 83: 140−144.

[4] PIERSON J F, THOBOR-KECK A, BILLARD A. Cuprite, paramelaconite and tenorite films deposited by reactive magnetron sputtering [J]. Applied Surface Science, 2003, 210: 359−367.

[5] YU Qing-chun, ZHANG Shi-chao, YANG Bin. Dispersion of copper oxide supported on γ-alumina and its sulfation properties [J]. Transactions of Nonferrous Metals Society of China, 2011, 21(12): 2644−2648.

[6] ZHAO Yue-qing, ZHAO Hai-lei, LIANG Ying-hua, JIA Qian-yi, ZHANGB Bo-bo. Preparation and characterization of CuO−CoO−MnO/SiO_2 nanocomposite aerogels as catalyst carriers [J]. Transactions of Nonferrous Metals Society of China, 2010, 20(8): 1463−1469.

[7] YAO Mao-hai, TANG You-gen, ZHANG Li, YANG Hai-hua, YAN Jian-hui. Photocatalytic activity of CuO towards HER in catalyst from oxalic acid solution under simulated sunlight irradiation [J]. Transactions of Nonferrous Metals Society of China, 2010, 20(10): 1944−1949.

[8] AI Z, ZHANG L, LEE S, HO W. Interfacial hydrothermal synthesis of Cu@Cu_2O core−shell microspheres with enhanced visible-light-driven photocatalytic activity [J]. The Journal of Physical Chemistry C, 2009, 113: 20896−20902.

[9] WANG S, XU H, QIAN L, JIA X, WANG J, LIU Y, TANG W. CTAB-assisted synthesis and photocatalytic property of CuO hollow microspheres [J]. Journal of Solid State Chemistry, 2009, 182: 1088−1093.

[10] AKHAVAN O, AZIMIRAD R, SAFA S, HASANI E. CuO/$Cu(OH)_2$ hierarchical nanostructures as bactericidal photocatalysts [J]. Journal of Materials Chemistry, 2011, 21: 9634−9640.

[11] LI Y, YANG X Y, ROOKE J, TENDELOO G V, SU B L. Ultralong $Cu(OH)_2$ and CuO nanowire bundles: PEG200-directed crystal growth for enhanced photocatalytic performance [J]. Journal of Colloid and Interface Science, 2010, 348: 303−312.

[12] LIU J, JIN J, DENG Z, HUANG S Z, HU Z Y, WANG L, SU B L. Tailoring CuO nanostructures for enhanced photocatalytic property [J]. Journal of Colloid and Interface Science, 2012, 384: 1−9.

[13] SOHRABNEZHAD S, MEHDIPOUR MOGHADDAM M J, SALAVATIYAN T. Synthesis and characterization of CuO–montmorillonite nanocomposite by thermal decomposition method and antibacterial activity of nanocomposite [J]. Spectrochimica Acta (Part A): Molecular and Biomolecular Spectroscopy, 2014, 125: 73−78.

[14] PASCHOALINO M, GUEDES N C, JARDIM W, MIELCZARSKI E, MIELCZARSKI J A, BOWEN P, KIWI J. Inactivation of *E. coli* mediated by high surface area CuO-accelerated by light irradiation >360 nm [J]. Journal of Photochemistry and Photobiology A: Chemistry, 2008, 199: 105−111.

[15] AKHAVAN O, GHADERI E. Cu and CuO nanoparticles immobilized by silica thin films as antibacterial materials and photocatalysts [J]. Surface and Coatings Technology, 2010, 205: 219−223.

[16] CHEN Han, FENG Fan, HU Zhong-liang, LIU Fu-sheng, GONG Wen-qiang, XIANG Kai-xiang. Preparation of uniform flower-like

CuO and flower-like CuO/graphene composite and their application in lithium ion batteries [J]. Transactions of Nonferrous Metals Society of China, 2012, 22(10): 2523−2528.

[17] AKHAVAN O, GHADERI E. Copper oxide microflakes as highly sensitive and fast response self-sterilizing biosensors [J]. Journal of Materials Chemistry, 2011, 21: 12935−12940.

[18] NARSINGA RAO G, YAO Y D, CHEN J W. Evolution of size, morphology, and magnetic properties of CuO nanoparticles by thermal annealing [J]. Journal of Applied Physics, 2009, 105: 093901.

[19] LIN X Z, LIU P, YU J M, YANG G W. Synthesis of CuO nanocrystals and sequential assembly of nanostructures with shape-dependent optical absorption upon laser ablation in liquid [J]. The Journal of Physical Chemistry C, 2009, 113: 17543−17547.

[20] SU Y K, SHEN C M, YANG H T, LI H L, GAO H J. Controlled synthesis of highly ordered CuO nanowire arrays by template-based sol−gel route [J]. Transactions of Nonferrous Metals Society of China, 2007, 17: 783−786.

[21] AKHAVAN O. Chemical durability of metallic copper nanoparticles in silica thin films synthesized by sol–gel [J]. Journal of Physics D: Applied Physics, 2008, 41: 235407.

[22] WANG J, HE S, LI Z, JING X, ZHANG M, JIANG Z. Self-assembled CuO nanoarchitectures and their catalytic activity in the thermal decomposition of ammonium perchlorate [J]. Colloid and Polymer Science, 2009, 287: 853−858.

[23] BAYANSAL F, ÇETINKARA H A, KAHRAMAN S, ÇAKMAK H M, GÜDER H S. Nano-structured CuO films prepared by simple solution methods: Plate-like, needle-like and network-like architectures [J]. Ceramics International, 2012, 38: 1859−1866.

[24] CHEN K, XUE D. Room-temperature chemical transformation route to CuO nanowires toward high-performance electrode materials [J]. The Journal of Physical Chemistry C, 2013, 117: 22576−22583.

[25] MUKHERJEE N, SHOW B, MAJI S K, MADHU U, BHAR S K, MITRA B C, KHA G G, MONDAL A. CuO nano-whiskers: Electrodeposition, Raman analysis, photoluminescence study and photocatalytic activity [J]. Materials Letters, 2011, 65: 3248−3250.

[26] WANG C, LI Q, WANG F, XIA G, LIU R, LI D, LI N, SPENDELOW J S, WU G. Morphology-dependent performance of CuO anodes via facile and controllable synthesis for lithium-ion batteries [J]. ACS Applied Materials & Interfaces, 2013, 6: 1243−1250.

[27] BARRECA D, GASPAROTTO A, MACCATO C, TONDELLO E, LEBEDEV O I, van TENDELOO G. CVD of copper oxides from a *β*-diketonate diamine precursor: Tailoring the nano-organization [J]. Crystal Growth & Design, 2009, 9: 2470−2480.

[28] DONG T Y, CHEN C N, CHENG H Y, CHEN C P, JHENG N Y. Controlled morphologies of copper oxide single crystalline nanostructures by wet chemistry and thermal decomposition processes [J]. Inorganica Chimica Acta, 2011, 367: 158−165.

[29] SAFARIFARD V, MORSALI A. Sonochemical syntheses of a nano-sized copper(II) supramolecule as a precursor for the synthesis of copper(II) oxide nanoparticles [J]. Ultrasonics Sonochemistry, 2012, 19: 823−829.

[30] AIMABLE A, TORRES PUENTES A, BOWEN P. Synthesis of porous and nanostructured particles of CuO via a copper oxalate route [J]. Powder Technology, 2011, 208: 467−471.

[31] BIGDELI F, MORSALI A. Synthesis ZnO nanoparticles from a new zinc(II) coordination polymer precursor [J]. Materials Letters, 2010, 64: 4−5.

[32] MASOOMI M Y, MORSALI A. Applications of metal–organic coordination polymers as precursors for preparation of nano-materials [J]. Coordination Chemistry Reviews, 2012, 256: 2921−2943.

[33] HANIFEHPOUR Y, MIRTAMIZDOUST B, JOO S. Sonochemical synthesis and characterization of the first flower-like cadmium(II) coordination compound: New precursor to produce pure phase nano-sized cadmium(II) oxide [J]. Journal of Inorganic and Organometallic Polymers and Materials, 2012, 22: 549−553.

[34] SOARES-SANTOS P C R, SÁ FERREIRA R A, TRINDADE T, CARLOS L D, NOGUEIRA H I S. Terbium(III) complexes of 2-aminonicotinic, thiosalicylic and anthranilic acids: Synthesis and photoluminescence properties [J]. Journal of Alloys and Compounds, 2008, 451: 575−577.

[35] ABU-YOUSSEF M A M, DEY R, GOHAR Y, MASSOUD A A A, ÖHRSTRÖM L, LANGER V. Synthesis and structure of silver complexes with nicotinate-type ligands having antibacterial activities against clinically isolated antibiotic resistant pathogens [J]. Inorganic Chemistry, 2007, 46: 5893−5903.

[36] MONICA T, AGUSTÍN S, MARÍA S G T, JOSÉ S C, JOSÉ S, EDUARDO E C, JAVIER E. Crystallographic report: Supramolecular structure of 2-aminonicotinatodimethylthallium (III), $[TlMe_2(2anic)]_n$ [J]. Applied Organometallic Chemistry, 2004, 18: 302−303.

[37] NAKAMOTO K. Infrared and Raman spectra of inorganic and coordination compounds: Part B [M]. 6th ed. New Jersey: Wiley, 2009.

[38] HOLLAND P L, TOLMAN W B. Three-coordinate Cu(II) complexes: Structural models of trigonal-planar type 1 copper protein active sites [J]. Journal of the American Chemical Society, 1999, 121: 7270−7271.

[39] SUN S, WANG W, ZHANG L, ZHOU L, YIN W, SHANG M. Visible light-induced efficient contaminant removal by Bi_5O_7I [J]. Environmental Science & Technology, 2009, 43: 2005−2010.

[40] GANDHI S, SUBRAMANI R H, RAMAKRISHNAN T, SIVABALAN A, DHANALAKSHMI V, NAIR M R G, ANBARASAN R. Ultrasound assisted one pot synthesis of nano-sized CuO and its nanocomposite with poly(vinyl alcohol) [J]. Journal of Materials Science, 2010, 45: 1688−1694.

[41] BAYANSAL F, KAHRAMAN S, ÇANKAYA G, ÇETINKARA H A, GÜDER H S, ÇAKMAK H M. Growth of homogenous CuO nano-structured thin films by a simple solution method [J]. Journal of Alloys and Compounds, 2011, 509: 2094−2098.

[42] SHAO Q, WANG L Y, WANG X J, YANG M C, GE S S, YANG X K, WANG J X. Hydrothermal synthesis and photocatalytic property of porous CuO hollow microspheres via PS latex as templates [J]. Solid State Sciences, 2013, 20: 29−35.

[43] KHATAEE A, AKBARPOUR A, VAHID B. Photoassisted electrochemical degradation of an azo dye using Ti/RuO_2 anode and carbon nanotubes containing gas-diffusion cathode [J]. Journal of the Taiwan Institute of Chemical Engineers, 2014, 45: 930−936.

[44] DEL C M, MALDONADO C, CAMPO T, ELIZALDE E, GOMEZ-MARTINEZ A, MORANT C, MARQUEZ F. Photocatalytic degradation of rhodamine-B under UV−visible light irradiation using different nanostructured catalysts [J]. American Chemical Science Journal, 2013, 3: 178−202.

[45] DANESHVAR N, RABBANI M, MODIRSHAHLA N, BEHNAJADY M A. Critical effect of hydrogen peroxide concentration in photochemical oxidative degradation of C.I. Acid Red 27 (AR27). [J]. Chemosphere, 2004, 56: 895−900.

以双(2-氨基烟酸)铜(II)微晶片为原料制备介孔结构 CuO 纳米颗粒的光催化性能

Azadeh TADJARODI [1], Omid AKHAVAN [2,3], Keyvan BIJANZAD[1]

1. Research Laboratory of Inorganic Materials Synthesis, Department of Chemistry, Iran University of Science and Technology, Tehran 16846-13114, Iran;
2. Department of Physics, Sharif University of Technology, Tehran 11155-9161, Iran;
3. Institute for Nanoscience and Nanotechnology, Sharif University of Technology, Tehran 14588-89694, Iran

摘　要：基于铜络合物的分解性质，提出一种制备具有介孔结构 CuO 纳米颗粒的简易方法。通过 2-氨基烟酸(Hanic)与硝酸铜(II)反应，制备一种具有微晶片行貌的新型铜络合物[Cu(anic)$_2$]·0.75H_2O(anic=2-氨基烟酸根)。元素分析和傅里叶红外光谱(FTIR)分析结果表明，该铜络合物的化学组成为 $CuC_{12}H_{11.5}N_4O_{4.75}$。铜络合物在 550 °C 烧结 4 h 后由微晶片结构转变为具有介孔结构的 CuO 纳米颗粒。经烧结过程后，铜络合物中归属于 2-氨基烟酸盐的 FTIR 吸收峰完全消失，证明形成了 CuO。XRD 分析结果亦证明生成了 CuO 纯晶。SEM 结果表明，CuO 纳米颗粒的平均晶粒尺寸为 75 mm。CuO 纳米颗粒的漫反射光谱分析结果表明，其带隙能约为 1.58 eV。在 H_2O_2 存在及经光照射 5 h 后，CuO 纳米颗粒对罗丹明 B 的催化降解率达到 100%。以上结果表明，所制得的 CuO 纳米颗粒是一种用于水处理的高效光催化剂。

关键词：氧化铜；纳米结构；2-氨基烟酸；光催化剂；热分解；降解率

(Edited by Wei-ping CHEN)